

A&A manuscript no.

(will be inserted by hand later)

Your thesaurus codes are:

06(08.01.1; 08.03.1; 08.05.3; 08.16.4)

ASTRONOMY  
AND  
ASTROPHYSICS

# A homogeneous study of the s-process in the 21 $\mu\text{m}$ carbon-rich post-AGB objects. <sup>\*</sup>

Hans Van Winckel<sup>1\*\*</sup> and Maarten Reyniers<sup>1\*\*\*</sup>

Instituut voor Sterrenkunde, K.U.Leuven, Celestijnenlaan 200B, B-3001 Leuven, Belgium

Received 2 July 1999 / Accepted 21 Sept. 1999

**Abstract.** We present in this paper a homogeneous photospheric abundance study, on the basis of the analysis of high resolution optical spectra, of six post-AGB objects displaying a 21 $\mu\text{m}$  circumstellar dust feature in their IR spectrum. The F-G spectral type of the 21 $\mu\text{m}$  stars make that a large range of elements including a wide variety of s-process elements, can be studied by their atomic lines. The high C/O-ratios together with the large overabundance of s-process elements prove that the objects are descendants of field carbon stars. We discuss in detail the s-process abundance distribution displayed by these 21 $\mu\text{m}$  stars and conclude that the 3rd dredge-up efficiency is closely related to the strength of the integrated neutron irradiation. The expected anti-correlation of the neutron irradiation with metallicity, on the other hand, contains a large *intrinsic* scatter. Finally we compare our results with other intrinsic and extrinsic s-process enriched objects and conclude that the post-AGB stars offer very useful complementary data to constrain the evolutionary models of AGB nucleosynthesis and dredge-up processes.

**Key words:** Stars: abundances; carbon; evolution; AGB and post-AGB

## 1. Introduction

A sub-class of post-AGB objects display in their IR spectrum an emission feature at 21 $\mu\text{m}$ , first identified on IRAS LRS spectra by Kwok et al. (1989). It was realised that the feature only occurs in spectra of C-rich post-AGB stars as evidenced by the presence of PAH-emission in the mid-IR spectra and often strong HCN measurements. The car-

rier(s) of the 21 $\mu\text{m}$  feature is (are) still unidentified. Its excitation and/or formation is limited to a short evolutionary phase since the feature is not observed in IR spectra of AGB stars nor in those of planetary nebulae (e.g. Kwok et al. 1999; Volk et al. 1999). The carbon rich nature of the circumstellar environment of these objects was corroborated by the detection of C<sub>2</sub>, C<sub>3</sub> and CN bands in the optical spectra (Hrivnak 1995). Detailed analysis of high-resolution spectra of these bands indicates that they are formed in a relatively narrow shell in the circumstellar envelope (Bakker et al. 1996; 1997).

Several studies of the photospheric composition confirmed the post-3rd dredge-up character of individual 21 $\mu\text{m}$  stars: they do not only display a high photospheric C/O ratio but also a large overabundance of s-process elements (Van Winckel 1999 and references therein). The colour-temperature of the IR-excess, the high luminosity and actual spectral type together with the chemical composition of both the photosphere and circumstellar material are all observational evidence that the 21 $\mu\text{m}$  stars are *post-carbon stars*.

Although in recent years the efforts and results on the theoretical modelling of the structural and chemical evolutionary AGB models are impressive (see e.g. Straniero et al. 1995; Frost & Lattanzio 1996; Herwig et al., 1997; Mowlavi et al. 1998; Mowlavi 1999; Langer et al. 1999) the calculations are not only dependent on fundamental parameters like initial mass and metallicity, but also on much less constrained or even free parameters like mass-loss history and geometry, details of the dredge-up phenomena and thermal pulse nucleosynthesis, numerical treatment of convection, interpulse phase at which the post-AGB phase starts, engulfed proton profile into the intershell, etc.

There is now general agreement that the neutrons, needed for the s-process nucleosynthesis in AGB stars, are mainly produced by the <sup>13</sup>C( $\alpha$ ,n)<sup>16</sup>O reaction with a possible contribution from the minor activation of the reaction <sup>22</sup>Ne( $\alpha$ ,n)<sup>25</sup>Mg (e.g. Smith & Lambert 1986; Jorissen & Arnould 1989; Busso et al 1992; Gallino et al 1998;

Send offprint requests to: Hans Van Winckel, e-mail: Hans.VanWinckel@ster.kuleuven.ac.be.

<sup>\*</sup> based on observations collected at the European Southern Observatory in Chile (61.E-0426), and at Roque de los Muchachos at La Palma Spain

<sup>\*\*</sup> Postdoctoral fellow of the Fonds National de la Recherche Scientifique

a primary source of  $^{13}\text{C}$ . This  $^{13}\text{C}$  pocket is naturally build up after engulfment of free protons into the  $^{12}\text{C}$ -rich intershell. The engulfed proton profile is, however, still a free parameter in the predictions. Straniero et al. (1995) proposed that the s-process synthesis occurs during the intershell in a radiative environment and they computed that the neutron irradiation varies within the radiative intershell depending on the engulfed proton profile.

The observational data guiding the theoretical chemical evolutionary models come from the analysis of intrinsic AGB stars of the M-MS-S-SC-C star sequence, (e.g. Lambert et al. 1995 and references therein) which is thought to reflect, at least partly, the evolution on the AGB of single stars towards an increasing C/O ratio. In addition, the enrichment in  $^{12}\text{C}$  seems to correlate well with an increase in s-process abundances (e.g. Smith & Lambert 1990). The study of the abundance distribution of different s-process elements is therefore a very useful tool to characterise the internal nucleosynthesis during and in between thermal pulses and to confine models of chemical evolution on the AGB. The strong molecular opacity and sometimes unstable photospheres of AGB stars make a quantitative analysis, however, difficult and some species even untraceable.

A second group of objects with excess abundances of s-process elements is the Ba-stargroup. In the rest of the paper we use the Ba-stargroup as a generic term for all objects for which the excess is acquired by mass-transfer from the companion which is now a white dwarf. It includes strong and mild Ba giants and Ba dwarfs, CH giant and subgiants, extrinsic S stars and since recently also yellow symbiotics (e.g. review by Jorissen 1999). The characteristics of the s-process excesses in these stars reflect the internal chemical enrichment of the companion, and the abundances may have been diluted by mixing of unprocessed material during the evolution of the gainer. The S-type stars in this group are normally labeled extrinsic S-stars and are characterised by the lack of Tc in their atmospheres (e.g. Jorissen et al. 1993) or their lower luminosity than intrinsic AGB S-stars (Van Eck et al. 1998).

In this paper, we analyse another group of intrinsic s-process enriched objects, namely the  $21\mu\text{m}$  stars. With their F to G spectral types, a wide variety of chemical species can be studied quantitatively by using photospheric atomic lines. This makes them ideal complementary sources to constrain the 3rd dredge-up nucleosynthesis and dredge-up models.

The chemical composition of individual  $21\mu\text{m}$  objects is already reported in the literature (Klochova 1995; Začs et al. 1995; Van Winckel et al. 1996a; Reddy et al. 1997; Decin et al. 1998, Klochkova et al. 1999). Since the different authors use different line-lists, spectral resolution and atomic data, it is often difficult to compare the results quantitatively. We therefore present in this paper a

the different s-process elements and the integrated neutron irradiation. In Sect. 2 we give an overview on the data obtained and sketch the reduction method, while the details of the chemical analysis are given in Sect. 3. In Sect. 4 a synopsis of our abundance analysis is presented proving that the  $21\mu\text{m}$  stars show clear chemical evidence for their post-AGB character. Sect. 5 is devoted to the discussion of the results of the individual objects and in Sect. 6 we focus on the heavy-element nucleosynthesis and the determination of the neutron exposure. Our findings on the post-AGB stars are then compared in Sect. 7 to the s-process abundances displayed in intrinsic AGB stars and extrinsic heavy-element enriched objects with a wide range in metallicity. We end with formulating the main conclusions in Sect. 8.

## 2. Observations and reduction

In Table 1 we list the sample of  $21\mu\text{m}$  stars discussed here together with the spectral domain observed and signal-to-noise obtained. Most spectra were obtained using the Utrecht Echelle Spectrograph (UES) mounted on the 4.2m William Herschel Telescope (WHT) on La Palma, Spain. We used the echelle with 31.6 lines/mm and the projected slit width was  $1.1''$  on the sky yielding a resolution of around  $R = \lambda/\delta\lambda \sim 50\,000$  depending on the wavelength.

Some of the UES spectra were kindly provided by Dr. Eric Bakker and used by him in his analysis of the optical circumstellar molecular absorption bands (Bakker et al. 1996; 1997). For IRAS07134 the 3.5m New Technology Telescope (NTT) of the European Southern Observatory (ESO) was used in combination with the high-resolution echelle mode of EMMI using grating number 14. The projected slit width was  $1''$  on the sky, yielding a resolution of  $R \sim 60\,000$ . Since most objects are heavily reddened, the S/N achieved depends strongly on wavelength and of course on the specific characteristics of the cross-dispersed spectrographs. The standard reduction included bias correction, flat-fielding, cosmic hits identification and cleaning and background subtraction. The extraction was done by a simple mean over the spatial profile and the wavelength calibration was performed by using Thorium-Argon lamp measurements. The different orders do not overlap from  $\sim 580\text{ nm}$  red-wards for the UES in combination with the  $1024^2$  pixel TEK CCD and for  $742\text{ nm}$  red-wards for EMMI with the  $2048^2$  TEK CCD (ESO number 36). We normalised the spectra by dividing the individual orders by a smoothed spline function defined through interactively identified continuum points. We used the specific echelle context of MIDAS for the reduction.

## 3. Analysis

**Table 1.** The programme stars: magnitude, coordinates, log of the observations and radial velocities.

IRAS	Other name	Visual magnitude m(v)	Equatorial coordinates		Galactic coordinates	
			$\alpha_{2000}$	$\delta_{2000}$	l	b
04296+3429		14.2	04 32 56.6	+34 36 11	166.24	-9.05
05341+0852		12.8	05 36 54.2	+08 54 10	196.19	-12.14
07134+1005	HD 56126	8.3	07 16 10.2	+09 59 47	206.75	+9.99
19500-1709	HD 187885	9.2	19 52 52.7	-17 01 50	23.98	-21.04
22223+4327		9.7	22 24 30.7	+43 43 03	96.75	-11.56
23304+6147		13.1	23 32 45.0	+62 03 49	113.86	+0.59
	Date and UT	Telescope+ Spectrograph	Sp. Range. (nm)	S/N	$v_{\text{helio}}$ (km s <sup>-1</sup> )	$v_{\text{LSR}}$ (km s <sup>-1</sup> )
04296+3429	22/2/1994 21:20	WHT+UES	556.5-1022	80	-53	-60
05341+0852	08/8/1995 05:15	WHT+UES	556.5-1004	50	24	8
07134+1005	29/9/1998 09:01	NTT+EMMI	398-662	blue : 160 green : 210	86	71
	24/2/1992 21:57	WHT+UES	535-1040	100	84	70
19500-1709	06/8/1995 23:55	WHT+UES	364-458	140	12	24
	08/8/1995 00:17	WHT+UES	453-680	240	13	25
	07/8/1995 01:34	WHT+UES	551-1004	320	12	24
22223+4327	23/8/1994 01:56	WHT+UES	443.5-650.5	180	-42	-30
	21/8/1994 22:45	WHT+UES	556.5-1004	190	-42	-30
23304+6147	23/8/1994 03:48	WHT+UES	443.5-650.5	50	-26	-16
	22/8/1994 01:09	WHT+UES	556.5-1004	110	-26	-16

line lists of the Vienna Atomic Line Database (VALD2, <http://www.astro.univie.ac.at/~vald/>, Kupka et al. 1999) were used, and estimated line strengths were computed. Next, the lines stronger than our detection limit were identified in the measured spectra.

The oscillator strengths ( $\log(gf)$ -values) were taken from several sources: for Fe, we used the critical compilation of Lambert et al. (1996), completed with values of Blackwell et al. (1980) for Fe II. Values for C, N and O were mainly taken from the Opacity Project (Hibbert et al. 1991, 1993; Biémont et al. 1991); values for the s-process elements from the Vienna Atomic Line Database (VALD2); values for the other elements mainly from Thévenin (1989, 1990), but also from Wiese et al. (1966), Reader et al. (1980), Fuhr et al. (1988), Martin et al. (1988), Venn (1995) and Gonzalez et al. (1997). The line list can be obtained from the authors upon request.

### 3.2. Radial velocities

The heliocentric radial velocities of the objects are given in Table 1 with an internal accuracy of  $\sim 1$  km s<sup>-1</sup>. Comparison with published velocities reveals no significant variability in most objects (see Table 2). For IRAS04296, an accurate velocity is hampered by our lower signal-to-noise. IRAS19500 and IRAS23304 are clearly not variable. For IRAS05341 and IRAS22223 we have not enough velocities to compare with, but non-variability is most likely

monitoring campaign, which spanned 440 days. They deduced radial velocity variations between 81.73 and 91.79 km s<sup>-1</sup> for this pulsating star but did not find evidence for binary motion. The measurement of Parthasarathy et al. (1992) deviates significantly from this range but it is difficult to evaluate since they do not give the date of observation. From the reception date of the article itself, it could have been very well during the monitoring campaign of Lèbre et al.

We can conclude that for none of the stars there is evidence for binarity from the radial velocities obtained so far.

### 3.3. Determination of atmospheric parameters and abundances.

In order to calculate abundances, we used the model atmospheres of Kurucz (1993) on his CDROM nr. 13. These LTE atmospheres are uniquely determined by the effective temperature ( $T_{\text{eff}}$ ), gravity ( $\log g$ ) and overall metallicity ( $Z$ ). The models were computed using opacity distribution functions assuming a constant microturbulent velocity ( $\xi_t$ ) of 2 km s<sup>-1</sup>.

The model parameters were based solely on the basis of the spectra, more specifically on the analysis of a set of well measured Fe I and Fe II lines with accurate atomic data. We used Fe for this purpose, not only because of the large number of lines, but also because of the accurate

**Table 2.** Heliocentric radial velocities of the programme stars, chronologically tabulated. The data used for the determination of the velocities include CO, and CS rotational line emission and optical spectra (opt.). The velocities we found are in bold. For these velocities, a detailed time indication can be found in Table 1, together with their value with respect to the Local Standard of Rest ( $v_{\text{LSR}}$ ).

IRAS	$v_{\text{helio}}$ ( $\text{km s}^{-1}$ )	method	date (mm/yy)	ref.
04296+3429	-55	CO	12/88	11
	-59	CO	01/89	7
	<b>-53</b>	opt.	02/94	
	-56	opt.	02/97	3
05341+0852	<b>24</b>	opt.	08/95	
	25	opt.	12/96	10
	26	CO	04/98	12
07134+1005	87	CO	01/89	7
	105	opt.	(?)	9
	82-92	opt.	01/91-04/92	5
	86	CO	04/90-01/91	1
	<b>84<sup>a</sup></b>	opt.	02/92	
	91	opt.	01/93	2
	86	opt.	12/93&02/94	8
19500-1709	<b>86<sup>b</sup></b>	opt.	09/98	
	13	CO	03/86	6
	13	CO	07/87	4
	13	CO	07/90	7
	12	CO	04/90-01/91	1
22223+4327	<b>12</b>	opt.	08/95	
	-37	CO	01/88	6
	-42	CO	01/89	7
23304+6147	<b>-42</b>	opt.	08/94	
	-26	CO	12/88	11
	-26	CO	01/88	6
	-26	CS	01/89	7
	<b>-26</b>	opt.	08/94	

(a) UES spectra (1992), (b) EMMI spectra (1998)

ref. (1) Bujarrabal et al. 1992 (2) Klochkova 1995 (3) Klochkova et al. 1999 (4) Knapp et al. 1989 (5) Lèbre et al. 1996 (6) Likkell et al. 1991 (7) Omont et al. 1993 (8) Oudmaijer & Bakker 1994 (9) Parthasarathy et al. 1992 (10) Reddy et al. 1997 (11) Woodsworth et al. 1990 (12) Hrivnak & Kwok 1999

face gravity  $\log g$  by demanding ionization equilibrium for Fe I and Fe II; the microturbulent velocity  $\xi_t$ , by forcing the abundances to be independent of the reduced equivalent widths  $\log(W_\lambda/\lambda)$ . Results of other authors or photometric data were used as a first guess. The stars in the sample are  $\sim 1000\text{ K}$  too cool to show He I-lines, so we could not obtain He abundances, except for the hottest star (IRAS19500,  $T_{\text{eff}}=8000\text{ K}$ ). We already reported the detection of a He I-line ( $\lambda 587.565\text{ nm}$ ) for this star in Van Winckel et al. (1996a). The obtained parameters are listed

**Table 3.** Model parameters of the six programme stars.

	Z	$T_{\text{eff}}$ (K)	$\log g$	$\xi_t$ ( $\text{km s}^{-1}$ )
IRAS04296	-0.5	7000	1.0	4.0
IRAS05341	-1.0	6500	1.0	3.5
IRAS07134	-1.0	7250	0.5	5.0
IRAS19500	-0.5	8000	1.0	6.0
IRAS22223	-0.5	6500	1.0	5.5
IRAS23304	-1.0	6750	0.5	3.0

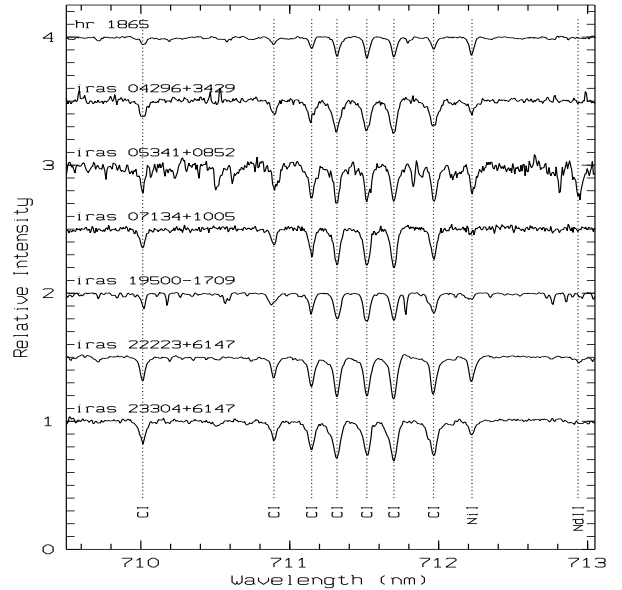


**Fig. 1.** Sample spectra of the programme stars around the red carbon multiplet. The stars are velocity corrected. On top, the spectrum of the reference star HR 1865 is plotted. This massive supergiant (F0Ib) has similar atmospheric parameters as the programme stars ( $T_{\text{eff}}=7500\text{ K}$ ,  $\log g=2.0$  and  $\xi_t=3.0\text{ km s}^{-1}$ , see Decin et al. (1998)) but obviously no enrichment of helium burning products.

and Van Winckel (1997) for an extensive error analysis and remind that the uncertainties, assuming LTE, are mainly induced by uncertain  $\log(gf)$  values and an uncertain temperature determination. Since the model atmospheres of Kurucz are listed with steps of  $\Delta T_{\text{eff}} = 250\text{ K}$  and  $\Delta \log(g) = 0.5$ , that correspond to the uncertainties of the spectroscopic parameter determinations, we did not interpolate between models. The possibility to infer an abundance of an ion critically depends on the presence of useful lines of that ion in the studied spectral range. We only used in this LTE analysis lines which appear unblended in our spectra and have an equivalent width smaller than  $150\text{ mÅ}$ .

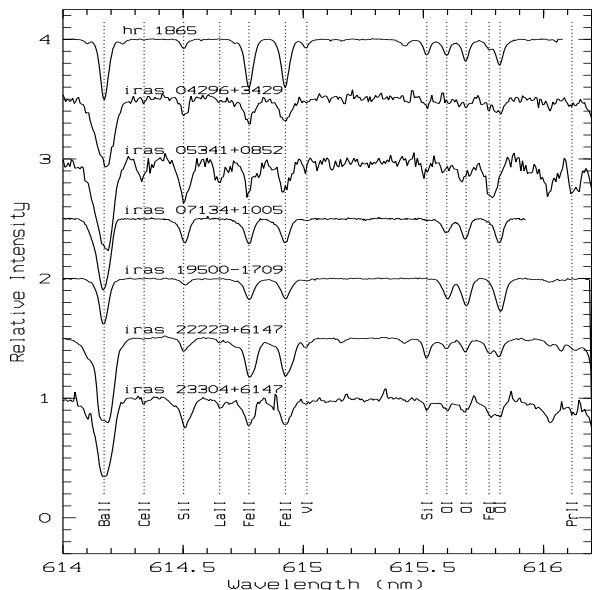


**Fig. 2.** Sample spectra of the programme stars and HR 1865 around the oxygen triplet at  $\lambda 615.6$  nm. For the cooler stars, a reliable oxygen abundance is rather problematic to derive, because of the small number of lines: only this multiplet is available for these stars. Hotter stars (IRAS07134 and IRAS19500) show more O lines. The equivalent width of the BaII-line exceeds our upper limit of  $150 \text{ m}\text{\AA}$  and can therefore not be used in a barium abundance calculation. A barium abundance is always difficult to determine because this element shows only a few very strong saturated lines and weak optical lines with  $W_\lambda < 150 \text{ m}\text{\AA}$  are very rare.

very consistent C-abundances ( $\sigma(\text{CI}) \leq 0.14$ , except for IRAS04296:  $\sigma(\text{CI}) = 0.20$ ). Useful nitrogen lines (NI) are more difficult to obtain, but there are some weak lines in the red part of the spectrum; only for IRAS07134 we measured more than 5 weak lines. The oxygen abundances of the  $21\mu\text{m}$  stars are in most cases more difficult to obtain. Since the O triplet at  $\lambda 777.4 \text{ nm}$  is strongly non-LTE sensitive, weaker lines should be used. For the cooler stars in the sample, only the high excitation multiplet at  $615.6 \text{ nm}$  can be used (Fig. 2), but since these lines are heavily blended, we used multiple Gaussian fitting to estimate their equivalent widths. For the two hotter stars IRAS07134 and IRAS19500, there are more lines in the spectrum, so the O-abundance is better established.

From sodium (Na,  $Z=11$ ) to sulphur (S,  $Z=16$ ), abundances are hard to obtain due to the lack of lines. Only two different sodium lines were found in the spectra ( $\lambda 568.265 \text{ nm}$  and  $\lambda 568.822 \text{ nm}$ ), both of them having

dance calculation. Silicon (Si) has more lines, but it shows for some stars a rather large line-to-line scatter.

For the heavier metals (Ca, Sc, Ti, Cr, Ni), more lines were found. Neutral calcium (Ca) is found in every star. Also scandium (Sc) and titanium (Ti) abundances were derived for almost every star, and this from lines of singly ionised atoms. Chromium (Cr) displays lines from neutral as well as singly ionised atoms, allowing an extra check for the ionization equilibrium (see Sect. 3.3). Nickel (Ni) is also found in every star, showing neutral lines in the cooler objects, ionised lines in the hotter ones. Other iron-peak elements found are vanadium (V), manganese (Mn) and zinc (Zn).

For the  $21\mu\text{m}$  stars which have F spectral types, the s-process elements are determined by lines from singly ionised atoms. The strontium (Sr) abundance is very difficult to determine accurately since the resonance lines at  $\lambda 421.5 \text{ nm}$  and  $\lambda 407.7 \text{ nm}$  are heavily saturated and weaker optical lines are not present. Yttrium (Y) and zirconium (Zr) abundances are more easily obtained. Moreover, these elements show a large number of lines in the hotter stars of our sample. An accurate barium (Ba) abundance is, like for Sr, difficult to determine, since weak optical lines are absent and only a few very strong saturated lines are present (for example, see Fig. 2). Three BaII-lines were found with  $W_\lambda < 150 \text{ m}\text{\AA}$ :  $\lambda 416.600 \text{ nm}$ ,  $\lambda 585.367 \text{ nm}$  and  $\lambda 873.776 \text{ nm}$ . Lanthanum (La), cerium (Ce) and neodymium (Nd) are easier to study and we obtained abundances for every star. Praseodymium (Pr) and samarium (Sm) have less lines and we were not able to determine abundances for these elements for every star. Also europium (Eu) lines are quite rare; we detected only three different EuII-lines in our spectra. Finally, we also detected a Hafnium (Hf,  $Z=72$ ) line ( $\lambda 409.316 \text{ nm}$ ) in the spectrum of IRAS07134 and IRAS19500 (Fig. 5). This line will be discussed in more detail in Sect. 5.

### 3.4. Hyperfine splitting

We investigated the influence of hyperfine splitting (hfs) on some observed lines which are considered to be sensitive for this effect. Hfs causes extra desaturation but is only important for lines of elements with an odd atomic number and strong nucleon-electron interaction.

Hfs will affect weak lines in their profile, but not in their equivalent width, leaving the derived abundance unchanged. For stronger lines on the flat part of the curve of growth, however, also the equivalent width will be affected. The hfs-influence critically depends on the temperature, since at higher temperatures the Doppler widths will wash out the effect of hfs on the line-profile.

The Kurucz spectrum synthesis program "Synthe" (Kurucz 1993) was used to study the influence of hfs. We

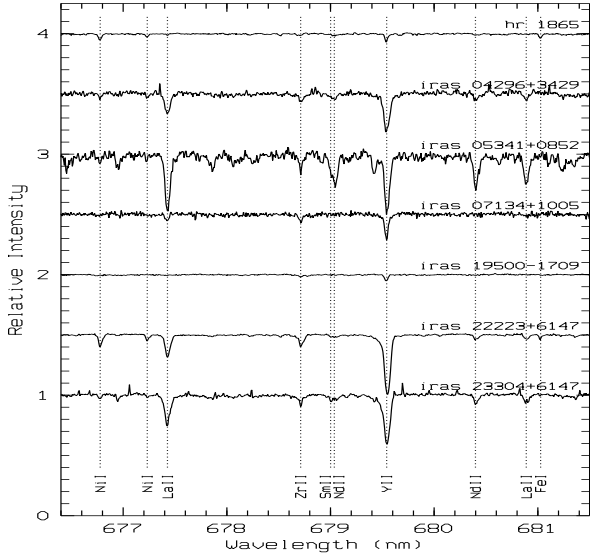


**Fig. 3.** The region around  $\lambda 679$  nm for the six programme stars and HR 1865. In this region, both lines of light s-process elements (ls) and of heavy s-process elements (hs) are present. Comparison with the normal supergiant HR 1865 proves that our stars are clearly s-process enhanced. The ratio of the line strength of the LaII-line at  $\lambda 677.427$  nm and the YII-line at  $\lambda 679.541$  nm for each star gives a first very qualitative idea of the neutron exposure (which is discussed in Sect. 6). In particular, from this comparison we can expect a high neutron exposure for IRAS05341.

ing lines which are considered to be among the most influenced by hfs-splitting: one aluminium ( $\lambda 394.401$  nm), one scandium ( $\lambda 660.460$  nm) and two europium lines ( $\lambda 412.973$  nm and  $\lambda 664.506$ ). The hsf-decompositions were obtained from McWilliam et al. (1995) and Biehl (1976).

The influence of hfs on  $W_\lambda$  of the synthetic lines was found to be noticeable, but spectrum synthesis made clear that the other sources of uncertainty (like continuum placement, errors on the atmospheric parameters etc.) are much more important in our programme stars. The small influence, even on the normally strongly affected Eu 412.973 nm line may surprise, but this line is only observed in the hotter stars where it has an equivalent width of only 32 mÅ at most. For the cooler  $21\mu\text{m}$  objects this line was not observed but our calculations indicate that this strong line would be heavily affected indeed.

Since line-profile fitting induces other uncertainties and since the effect on the weak lines used in our analysis is very small, we did not include hfs profile fitting

## 4. Synopsis of the abundance results

In this section we discuss Table 4 and Fig. 4, which give an overview of the results of our abundance analysis. In the last column of Table 4, we list a typical abundance pattern for an unevolved metal deficient star (e.g. Lambert 1989; Wheeler et al. 1989; Edvardsson et al. 1993; McWilliam 1997) reflecting the chemical composition of our programme stars at the time of their formation. Comparing these unprocessed abundances with the observed abundances permits us to detect possible changes in the chemical composition during the stars evolution. Applied to low-mass post-AGB stars, we expect the chemical signature of the 3rd dredge-up without activation of hot-bottom burning i.e. the enrichment of the stellar photosphere with material exposed to He-burning during the TP-AGB phase. This signature includes: carbon and (to a lesser extent) oxygen enrichment, a C/O number ratio higher than solar ( $C_\odot/O_\odot=0.51$ ) and, above all, s-process enrichment. All  $21\mu\text{m}$  sources studied here turn out to show almost all these enrichments, which make them a group of definite post 3rd dredge-up post-AGB stars.

### 4.1. Metallicity

To calculate the metallicity, we used the iron abundance inferred from the FeII-lines since this is by far the dominant ionization level. The metallicity relative to the solar value ranges from  $-0.3$  (IRAS22223) to  $-1.0$  (IRAS07134). This is a strong indication that our sample indeed consists of an old and hence low-mass population. This interpretation is further strengthened by the high galactic latitudes of the stars, in the range  $|b|=9^\circ-21^\circ$ . An exception with respect to the latter criterion is IRAS23304, for which  $b = 0.6^\circ$ . Its low-mass nature is, however, clear from the low metallicity ( $[Fe/H]=-0.8$ ).

### 4.2. CNO abundance

All stars display huge carbon-enrichments. This enrichment is beyond any doubt even when the internal scatter of the C-lines and the uncertainty induced by the model parameters are taken into account. As already pointed out in Sect. 3.3, the O-abundance is in most cases less certain. Only for the two hotter objects IRAS07134 and IRAS19500 we feel confident that we detected a moderate but real O-enrichment. The reliability of the oxygen abundances will be discussed in the following section, in which we treat the objects separately.

Unfortunately, the errors on mainly the O-abundance preclude accurate C/O number ratio determination based

**Table 4.** Synopsis of the abundance results. The  $[\alpha/\text{Fe}]$  value is the mean of the  $[\text{el}/\text{Fe}]$  values of the observed  $\alpha$ -elements Mg, Si, S, Ca and Ti;  $[\text{ls}/\text{Fe}]$  the mean of the  $[\text{el}/\text{Fe}]$  values of Sr, Y and Zr;  $[\text{hs}/\text{Fe}]$  the mean of  $[\text{el}/\text{Fe}]$  of Ba, La, Nd and Sm;  $[\text{s}/\text{Fe}]$  the mean of the former 7 s-process elements.

	IRAS	04296	05341	07134	19500	22223	23304	subdwarf
metallicity	[Fe/H]	-0.6	-0.8	-1.0	-0.6	-0.3	-0.8	-0.7
CNO abundance	[C/Fe]	0.8	1.0	1.1	1.0	0.3	0.9	0.0
	[N/Fe]	0.4	0.7	0.9	1.0	0.2	0.5	0.0
	[O/Fe]	/	0.6	0.8	0.7	-0.1	0.2	0.4
$\alpha$ -elements	$[\alpha/\text{Fe}]$	0.5	0.4	0.1	0.3	0.2	0.4	0.3
s-process elements	[s/Fe]	1.5	2.2	1.5	1.1	0.9	1.6	0.0
	[ls/Fe]	1.7	1.9	1.6	1.4	1.3	1.6	0.0
	[hs/Fe]	1.5	2.3	1.5	1.0	0.8	1.6	0.0

#### 4.3. $\alpha$ -elements

The  $[\alpha/\text{Fe}]$  value is the mean of the  $[\text{el}/\text{Fe}]$  values of the observed  $\alpha$ -elements. If we take into account a typical error of 0.2 dex in the abundances, we may conclude that the  $\alpha$ -overabundances reflect the chemical history of the Galaxy and are therefore not enhanced.

The  $\alpha$ -elements show, however, large differences in their  $[\text{el}/\text{Fe}]$  values within each star, up to an extreme value of 1 dex. Unfortunately, the lack of useful lines for the light  $\alpha$ -elements prevent too strong conclusions whether this is intrinsic or due to non-LTE effects and/or unaccurate  $\log(gf)$ . The  $[\alpha/\text{Fe}]$  value is therefore only an indicative number.

#### 4.4. s-process enrichment

The s-process elements observed in evolved stars can be divided into two groups: the light s-process elements around the magic neutron number 50 (Sr, Y, Zr) and the heavy s-process elements around the magic neutron number 82 (Ba, La, Ce, Pr, Nd, Sm, (Eu)). In order to investigate the s-process abundances in more detail, four indexes are generally defined:  $[\text{s}/\text{Fe}]$ ,  $[\text{ls}/\text{Fe}]$ ,  $[\text{hs}/\text{Fe}]$  and  $[\text{hs}/\text{ls}]$ . Which elements are taken into account to determine these indices is different from author to author and is mainly determined by the possibility to compute accurate abundances of the different elements. To compare the results on  $21\mu\text{m}$  stars with other s-process enriched objects, the same index should be used. We follow the proposition of Busso et al. (1995) and define the ls-index as the mean of Sr, Y and Zr and the hs-index as the mean of Ba, La, Nd and Sm. Consequently,  $[\text{s}/\text{Fe}]$  is the mean of the 7 former elements and  $[\text{hs}/\text{ls}] = [\text{hs}/\text{Fe}] - [\text{ls}/\text{Fe}]$ .

For unobserved species of the light s-process no correction factor was taken into account since the odd-even effect is not very strong. For unobserved species of the hs index, for which the odd-even effect is much stronger, the unde-

This method was used to estimate the Sm-abundance for IRAS04296 and IRAS19500. Note that the  $[\text{hs}/\text{ls}]$  index is by its definition in principle independent of the *total* s-process enrichment ( $[\text{s}/\text{Fe}]$ ).

Regarding Table 4, the overabundance of the s-process elements is beyond any doubt and is definitely the most convincing argument for the post 3rd dredge-up status of the studied stars. For unevolved objects in the same metallicity range, one expects the s-process elements to scale with Fe:  $[\text{s}/\text{Fe}] = 0$  (see Wheeler et al. 1989). Here we find  $[\text{s}/\text{Fe}] \geq 0.9$  (IRAS22223), up to  $[\text{s}/\text{Fe}] = 2.2$  (IRAS05341).

### 5. Individual objects

The individual objects will be discussed in this section. In Table 5 we list the complete abundance analysis of each programme star. We want to stress that we will not repeat the conclusions already made in the previous section, but that we will focus on the peculiarities in the analysis of each star.

#### 5.1. IRAS 04296+3429

The chemical analysis of this object has already been discussed by our group (Decin et al. 1998). Nevertheless, there are some minor differences between the present analysis and the previous one, as a consequence of an update of our line list. The main conclusions of Decin et al. (1998) remain valid.

#### 5.2. IRAS 05341+0852

This object was first mentioned by Geballe & Van der Veen (1990) suggesting that it is an evolved F-type supergiant displaying carbon-rich circumstellar dust. Its  $21\mu\text{m}$  feature was discovered by Kwok et al. (1995). An extensive abundance analysis was previously carried out by Reddy et al. (1997). They found the star to be metal-poor,

**Table 5.** Chemical analysis of the programme stars. For every ion we list the solar abundance and for every star the number of lines used (N), the equivalent width ( $\overline{W}_\lambda$ ), the abundance ratio relative to iron ([el/Fe]) and the internal scatter ( $\sigma$ ), if more than one line is used. For the solar iron abundance we used the meteoric iron abundance of 7.51. For the solar C, N and O abundances we adopted resp. 8.57, 7.99 and 8.86 (C: Biémont et al. 1991, Hibbert et al. 1991, O: Biémont et al. 1991); the other solar abundances are taken from Grevesse (1989). Note that abundances based on one line should be treated with caution.

		IRAS04296 [Fe/H]=−0.62				IRAS05341 [Fe/H]=−0.85				IRAS07134 [Fe/H]=−1.00				IRAS19500 [Fe/H]=−0.60				IRAS22223 [Fe/H]=−0.31				IRAS22223 [Fe/H]=−0.31	
ion	Solar	N	$\overline{W}_\lambda$	[el/Fe]	$\sigma$	N	$\overline{W}_\lambda$	[el/Fe]	$\sigma$	N	$\overline{W}_\lambda$	[el/Fe]	$\sigma$	N	$\overline{W}_\lambda$	[el/Fe]	$\sigma$	N	$\overline{W}_\lambda$	[el/Fe]	$\sigma$	N	$\overline{W}_\lambda$
He I	10.99																						
C I	8.57	7	87	+0.76	0.20	11	96	+1.01	0.14	40	58	+1.08	0.12	21	48	+1.01	0.12	8	70	+0.32	0.14	15	71
N I	7.99	2	65	+0.39	0.01	3	52	+0.69	0.08	8	84	+0.85	0.15	3	85	+0.98	0.11	4	54	+0.16	0.08	3	45
O I	8.86					2	31	+0.56	0.00	8	44	+0.81	0.11	8	62	+0.70	0.08	3	24	−0.05	0.04	4	15
Na I	6.33					1	26	+0.04		1	11	+0.46		1	10	+0.22						1	20
Mg I	7.58									1	71	+0.06		3	95	+0.24	0.18						
Mg II														4	48	+0.51	0.07						
Al I	6.47													1	95	−0.28		4	16	−0.01	0.10		
Si I	7.55	3	55	+0.79	0.26	5	50	+0.59	0.16									14	46	+0.29	0.14	5	39
Si II	7.21	1	57	+0.43		1	42	+0.28		1	15	+0.40		1	6	+0.26		4	53	+0.04	0.19	4	36
Ca I	6.36	3	35	+0.18	0.16	6	55	+0.08	0.18	5	21	−0.11	0.08	1	11	+0.49		6	57	−0.09	0.10	7	63
Ca II																		1	16	−0.25			
Sc II	3.10									6	50	+0.22	0.10	6	49	+0.38	0.15					2	110
Ti I	4.99																	2	26	+0.47	0.07		
Ti II						1	52	+0.58		31	84	+0.11	0.15	11	70	+0.19	0.15					3	111
V II	4.00									1	107	−0.05		1	97	+0.12							
Cr I	5.67									3	79	−0.15	0.13	3	50	+0.19	0.08	7	45	−0.08	0.15	1	5
Cr II										18	58	+0.19	0.13	20	51	+0.13	0.10	6	118	−0.03	0.23	2	40
Mn I	5.39																	1	38	−0.26			
Mn II										2	22	+0.16	0.05					1	50	+0.13		1	6
Fe I	7.51	8	32	−0.04	0.11	23	57	+0.05	0.14	36	32	−0.08	0.15	15	29	−0.05	0.06	41	57	−0.11	0.14	39	53
Fe II		10	74		0.10	7	84		0.14	17	67		0.10	18	74		0.06	12	49		0.15	7	63
Ni I	6.25	3	47	+0.54	0.11	7	45	+0.53	0.19	2	7	−0.12	0.11					19	35	−0.01	0.16	9	18
Ni II										1	31	−0.11		4	27	+0.11	0.15						
Zn I	4.60									1	15	+0.37											
Y II	2.24	3	84	+1.98	0.06	2	129	+2.09	0.02	16	79	+1.50	0.25	18	74	+1.34	0.18	4	128	+1.51	0.09	2	51
Zr II	2.60	4	33	+1.34	0.23	3	72	+1.75	0.15	19	59	+1.60	0.22	22	80	+1.41	0.11	5	83	+1.04	0.15	4	33
Ba II	2.13	1	25	+1.73		1	82	+2.43		1	53	+1.94		1	55	+1.48		1	13	+0.85		1	40
La II	1.22	5	59	+1.74	0.13	17	94	+2.47	0.17	31	28	+1.65	0.15	6	26	+1.21	0.09	16	68	+1.04	0.17	9	64
Ce II	1.55	2	24	+1.20	0.04	6	71	+2.40	0.14	50	43	+1.45	0.21	7	10	+0.91	0.13	8	52	+0.82	0.23	9	57
Pr II	0.71					16	69	+2.40	0.19	4	10	+1.45	0.11					5	48	+0.92	0.24	4	29
Nd II	1.50	2	23	+1.08	0.17	19	96	+2.47	0.19	29	19	+1.31	0.12	1	3	+0.52		12	51	+0.73	0.20	21	45
Sm II	1.00					4	71	+1.85	0.03	9	12	+1.04	0.05					10	53	+0.50	0.20	5	21
Eu II	0.51	1	41	+0.97		1	38	+1.22		1	30	+0.48		1	3	+0.26		2	47	+0.57	0.06	1	65
Hf II	0.88									1	83	+1.84		1	12	+1.25							



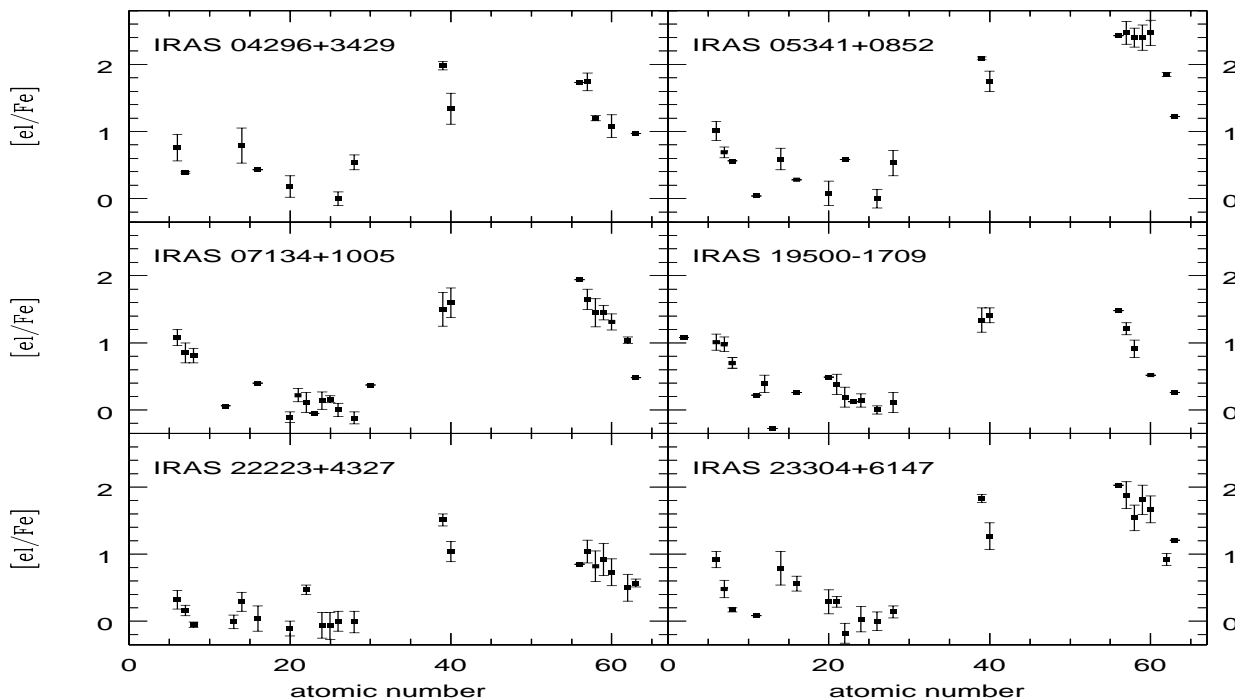


**Fig. 4.** The abundances of our six programme stars relative to iron  $[\text{el}/\text{Fe}]$ .

For the model parameters, we found  $T_{\text{eff}}=6500\text{K}$ ,  $\log g=1.0$  and  $\xi_t=3.5 \text{ km s}^{-1}$ . The model parameters agree with those found by Reddy (6500, 0.5, 5.0), but there are some differences in the abundances. In general, for species displaying a large difference, our analysis was based upon significantly more lines, which should imply that our results are intrinsically more reliable.

Besides the huge carbon enrichment also oxygen is moderately enhanced ( $[\text{O}/\text{Fe}]=+0.6$ ) but this value is based only on two blended lines.

Reddy et al. also found a significant overabundance of lithium and we confirm the presence of the Li line at  $\lambda 670.7\text{nm}$  in our spectra as well.

The number of lines of the s-process elements is impressive. A close look at the spectrum reveals that it is even completely dominated by lines of s-process elements.  $[\text{s}/\text{Fe}]$  (Table 4) is 2.2, making IRAS05341 the most s-process enhanced post-AGB star known so far. Note the even-odd alternation of the absolute abundances (Fig. 6) and the good internal consistency ( $\sigma < 0.20$ ). There is significant difference in the  $[\text{el}/\text{Fe}]$  ratios of our analysis and the one of Reddy et al. (1997) reaching up to +0.8 dex. Since we take much more and much weaker lines into account reaching a good internal accuracy, and use the

### 5.3. IRAS07134+1005 = HD 56126

With its 8.3 visual magnitude, this is the brightest star in our sample. Considerable efforts have been performed already to reveal the properties of the circumstellar shell of this well-known post-AGB star.  $^{12}\text{CO}$ ,  $^{13}\text{CO}$ , HCN and  $\text{HCO}^+$  (Bujarrabal et al. 1992, Omont et al. 1993) have been detected in millimeter and radio line emission. The  $21\mu\text{m}$  feature was discovered by Kwok et al. (1989) in its IRAS Low Resolution Spectrum. Optical spectra revealed the presence of circumstellar  $\text{C}_2$ ,  $^{12}\text{CN}$  and  $^{13}\text{CN}$  bands (Bakker et al. 1996; Bakker & Lambert 1998a) and  $^{12}\text{C}^{13}\text{C}$  and  $^{12}\text{C}^{16}\text{O}$  bands (Bakker & Lambert 1998b), which led to an estimate for the  $^{12}\text{C}/^{13}\text{C}$  ratio :  $^{12}\text{C}/^{13}\text{C} = 72 \pm 26$ . Mid-infrared (8- $21\mu\text{m}$ ) imaging shows no spherical but possibly an axial symmetry of the dust emission (Meixner et al. 1997; Dayal et al. 1998).

Concerning the *photosphere*, there is general agreement that IRAS07134 is a pulsating star, but different pulsation periods have been published (e.g. Lèbre et al. 1996). Limited abundance analyses have already been performed by Parthasarathy et al. (1992) and by Klochkova (1995), showing chemical evidence for the post-AGB status of this object. However, the high quality NTT-spectra for this star permitted us to elaborate a much more detailed abundance analysis. We used 342 lines of 27 different ions.

However, the latter author found a much larger abundance if deduced from lines of neutral atoms than from lines of singly ionized atoms of the same element. This was attributed to unknown non-LTE effects. We do not confirm this result since careful analysis of our much higher S/N spectra does not reveal the presence of most neutral lines, while we identified some lines differently. This illustrates that it is often very difficult to assign uncertain LTE abundance results of an individual object solely to non-LTE effects. Also the effect of other uncertainties should be carefully studied and a more systematic approach using data on several objects should be initiated to evaluate possible non-LTE deviations of specific lines.

The ionization equilibrium of Ni is also fulfilled but for Cr we find a  $\Delta(\log A(\text{CrII}) - \log A(\text{CrI})) = 0.34$ . A lower model gravity can solve this inconsistency for Cr but it may also indicate non-LTE occupation numbers for the different ions of Cr. We chose not to change our model parameters in order not to compromise significant comparison with the other stars in our sample.

A problem occurred when calculating the Fe abundance from lines of neutral iron with a very low excitation potential: the lines with a very small lower excitation potential gave systematically lower abundances. This is a strong indication that non-LTE over-excitation occurs. We therefore discarded all FeI-lines with an excitation potential  $\chi < 1.25\text{eV}$  in our abundance determinations, also for all other programme stars.

The large line-to-line scatter in the abundance of Y and Zr is solely caused by only three lines of Y ( $\lambda 578.169\text{nm}$ ,  $\lambda 550.990\text{nm}$  and  $\lambda 528.982\text{nm}$ ), and two lines of Zr ( $\lambda 448.545\text{nm}$  and  $\lambda 449.546\text{nm}$ ). These lines do not show any systematic trend with another atomic parameter (wavelength, excitation potential, equivalent width), so the anomalies are probably caused by inaccurate  $\log(gf)$ -values. The only line in common with the other stars is the YII-line at  $528.982\text{nm}$  in IRAS22223. Also for this star, the abundance inferred from this line is significantly lower than the abundances inferred from the other lines.

We also detected several lines of singly ionised Hafnium ( $Z=72$ ) in the blue part of the spectrum of IRAS07134, but only two of them turned out to be unblended ( $\lambda 409.316\text{nm}$ ,  $W_\lambda = 83\text{m}\text{\AA}$  and  $\lambda 466.414\text{nm}$ ,  $W_\lambda = 19\text{m}\text{\AA}$ ). Unfortunately, the Hf-abundance derived from these two lines differs by 0.4 dex ( $\log A(\text{Hf}) = 1.72$  and  $2.09$  respectively). These abundances are both very high if compared with the calculations of Malaney (1987). We expect  $\log A(\text{Hf}) \approx 1.1$  for a neutron exposure of  $\tau = 0.3\text{mb}^{-1}$  (neutron exposure: see Sect. 6). No other possible identification could, however, be found. An interpretation of this result is difficult, not only because of

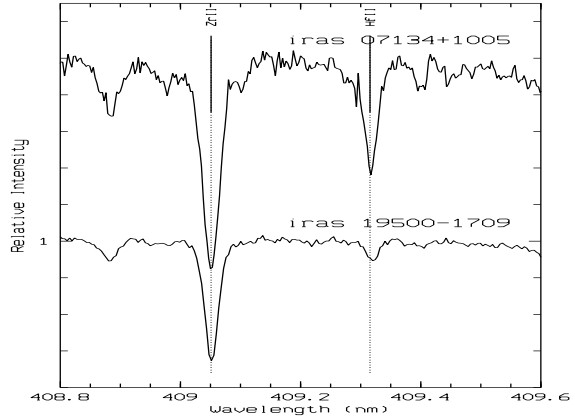


**Fig. 5.** The HfII-line ( $\lambda 409.316\text{nm}$ ) in the blue spectrum of IRAS07134 and IRAS19500. The derived hafnium abundance is quite high, but blends or a wrong identification is almost certainly excluded.

#### 5.4. IRAS 19500–1709 = HD 187885

This post-AGB candidate shows only a weak  $21\mu\text{m}$  feature (Justtanont et al. 1996) which is probably an effect of the higher temperature of this object. We already published an abundance analysis of this object (Van Winckel et al. 1996a) based on ESO La Silla spectra. The latter spectra show HeI lines at  $447.08\text{nm}$  and  $587.6\text{nm}$  pointing to a hot source. Indeed, demanding excitation equilibrium of the Fe I-lines yielded a temperature  $T_{\text{eff}}=8000\text{K}$ .

In this study we present a new analysis (Table 5) based on UES-spectra with a higher S/N and a broader spectral coverage. The analysis of the iron lines yielded the same atmospheric parameters, only the  $\log(W_\lambda/\lambda)$ -abundance diagram points to a larger microturbulent velocity  $\xi_t = 6\text{km s}^{-1}$ . The lines of the s-process elements Y and Zr favour a slightly lower value of  $\xi_t \leq 5\text{km s}^{-1}$ . We again keep the atmospheric parameters obtained using the iron lines. A change in the microturbulent velocity of  $\sim 1\text{km s}^{-1}$  will only influence the abundance deduced from the largest lines ( $W_\lambda \geq 120\text{m}\text{\AA}$ ) with a typical value of 0.1 dex.

Comparing this analysis with our previous one, there are some quantitative differences, but our conclusions for this star remain unchanged. The s-process overabundance is now much better established, with more lines for the ls-elements and new abundances for the hs-elements La, Ce, Nd and Eu.

We report also for this star the detection of a line of singly ionised Hafnium at  $\lambda 409.316\text{nm}$ . An equivalent width  $W_\lambda = 12\text{m}\text{\AA}$  gives an abundance of  $\log A(\text{Hf}) = 1.53$  which is again quite high if compared with the calculations of Malaney (1987). We expect  $\log A(\text{Hf}) \approx 1.0$  for a  $\tau = 0.2\text{mb}^{-1}$ . Another argument against such

should have an equivalent width of  $W_\lambda = 9 \text{ m}\text{\AA}$ . Inaccurate  $\log(gf)$ -values can be the cause of this inconsistency. Other possibly detectable Hf II lines are all heavily blended.

### 5.5. IRAS 22223+4327

The chemical composition of this star was recently discussed by Decin et al. (1998). We list the individual abundances here again since minor differences are obtained due to an upgrade of the line-list and a homogenization of the atomic data.

### 5.6. IRAS 23304+6147

Kwok et al. (1989) classified this object as a proto-planetary nebula and discovered its  $21\mu\text{m}$  feature. The circumstellar dust turned out to be C-rich as confirmed by several authors: detection of  $\text{C}_2$ ,  $\text{C}_3$  (Hrivnak 1995), CO, HCN (Omont et al. 1993), CN (Bakker et al. 1997) and non-detection of OH (Likkell 1989). Hrivnak et al. (1999) found the object to be resolved in V with an extent of about 2 arcsec. Reddy & Parthasarathy (1996) derived model parameters for this object by fitting a Kurucz model atmosphere through the observed spectral energy distribution. This technique yielded  $T_{\text{eff}}=5000\text{K}$  and  $\log g=1.0$ . Comparing our spectra with the other stars in our sample, we concluded that this temperature was probably too low : the high excitation O-triplet around  $\lambda 615.6\text{nm}$  is clearly detected (see Fig. 2). Indeed, also our spectroscopic determination of the temperature using the iron-lines resulted in a  $T_{\text{eff}}=6750\text{K}$ . The abundance analysis makes IRAS23304 join the group of post-AGB stars that clearly display chemical evidence of their post 3rd dredge-up character.

To our knowledge, this is the first detailed photospheric abundance study of this star. The internal scatter of the four O-lines is small indicating that the very high C/O ratio of 2.9 is probably real. For the metallicity, we find the value  $[\text{Fe}/\text{H}]=-0.8$ . The other iron peak elements do follow this deficiency. Again, the s-process abundances are quite impressive for this star. Note that the internal scatter of the different abundance determinations are somewhat higher for this star than for the other programme stars as a consequence of the lower S/N of our spectra ( $m_v=13.1$ ).

## 6. Neutron exposure of $21\mu\text{m}$ stars

### 6.1. Goodness-of-fit

A theoretical parameter describing the neutron irradiation is the neutron exposure rate  $\tau$  which is defined as

**Table 6.**  $S^2$  values for different neutron exposures  $\tau_0$  ( $N_n = 10^8 \text{cm}^{-3}$ ). The stars are listed with increasing [hs/lr]-value.

	$\tau_0 \text{ (mb}^{-1}\text{)}$					[hs/lr]
	0.1	0.2	0.3	0.4	0.5	
	0.6	0.7	0.8	0.9	1.0	
IRAS22223	1.55	<b>0.45</b>	0.55	0.76	0.95	-0.5
	1.11	1.23	1.35	1.44	1.51	
IRAS19500	1.29	<b>0.34</b>	0.70	1.09	1.42	-0.4
	1.65	1.85	2.03	2.17	2.27	
IRAS04296	2.35	0.80	<b>0.74</b>	0.89	1.05	-0.2
	1.18	1.28	1.39	1.48	1.54	
IRAS07134	1.95	0.61	<b>0.58</b>	0.73	0.88	-0.1
	0.99	1.10	1.19	1.26	1.32	
IRAS23304	3.36	1.17	0.76	<b>0.72</b>	0.75	+0.1
	0.78	0.82	0.87	0.91	0.94	
IRAS05341	4.09	1.28	0.60	0.39	0.31	+0.4
	0.29	<b>0.28</b>	<b>0.28</b>	0.29	0.30	

modelled by an exponential irradiation parameterized by a mean neutron exposure  $\tau_0$  (e.g. Ulrich 1973). In most calculations, the neutron density and the fraction of the inter-shell material that remains exposed to neutrons are adopted as constants. The efficiency of s-processing is then indicated by one parameter  $\tau_0$ .

The neutron exposure  $\tau_0$  is intimately related to the [hs/lr] index: a large  $\tau_0$  yields a large [hs/lr]. In order to estimate  $\tau_0$  quantitatively, we used the theoretical models of Malaney (1987) and the 'goodness of fit' procedure as defined by Cowley & Downs (1980). A description of this method can also be found in Vanture (1992) and Smith et al. (1996). In this method, the quantity  $S^2$  is defined as

$$S^2 = \frac{1}{N} \sum_{i=1}^N \frac{(O_i - (M_i + \delta))^2}{\sigma_i^2}$$

where  $N$  is the number of s-process elements involved in the comparison,  $O_i$  the observed abundance of element  $i$ ,  $M_i$  the predicted model abundance as tabulated by Malaney,  $\delta$  the average offset between the observed and the predicted s-process abundances ( $\delta = 1/N \sum_i (O_i - M_i)$ ) and  $\sigma_i$  is the uncertainty on the obtained individual abundance  $O_i$ .  $O_i$  and  $\sigma_i$  are calculated as described in Decin et al. (1998) so on top of the internal accuracy a fixed value of 0.3 was quadratically added to account for the uncertainties on the model atmosphere parameters and eventual systematic offsets in the  $\log(gf)$  values. The values for  $S^2$  for each model and each star are listed in Table 6. A graphical presentation of the best fit for two stars (IRAS07134 and IRAS05341) can be found in Fig. 6. Note that the  $S^2$  are small which indicates a good consistency between the abundances of different s-process

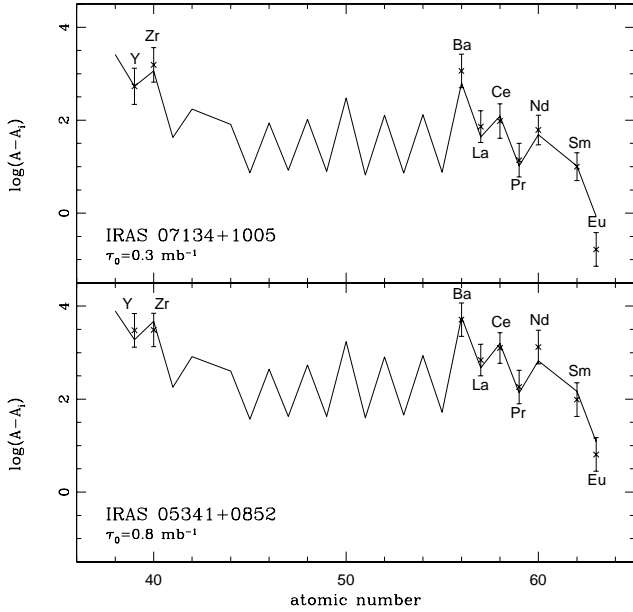


**Fig. 6.** Comparison of the observed abundances with the calculations of Malaney (1987) for IRAS07134 and IRAS05341. The observed abundances were corrected for the initial abundances ( $A_i$ ) assuming  $[s/Fe]_i=0$  (except for Eu). As evidenced by the 'goodness of fit' procedure, the s-process elemental distribution of IRAS07134 points to a rather moderate neutron exposure, whereas the distribution of IRAS05341 is best fitted by a large neutron exposure  $\tau_0 = 0.8 \text{ mb}^{-1}$ .

$S^2$  and so the neutron exposure  $\tau_0$  is well defined. For stars with a higher  $[hs/ls]$ , a larger range of values for  $\tau_0$  are possible: a high neutron exposure will only raise the overall level of enhancement without significantly changing the distribution of the individual abundances (see also Fig. 9). Therefore, the s-process distribution of IRAS05341 fits well for every  $\tau_0 \geq 0.5 \text{ mb}^{-1}$ .

### 6.2. Total s-process enrichment of $21\mu\text{m}$ stars.

In Fig. 7 the  $[hs/ls]$  index from the  $21\mu\text{m}$  stars is shown in comparison with the overall s-process enrichment as parameterised by the  $[s/Fe]$ -index. More objects should clearly be studied, but the total neutron exposure is surprisingly strongly correlated with the total enrichment of s-process elements in the  $21\mu\text{m}$  stars, with more enriched objects showing also a stronger total neutron irradiation! A simple linear least-squares fit gives a high correlation coefficient of +0.96 with the fit

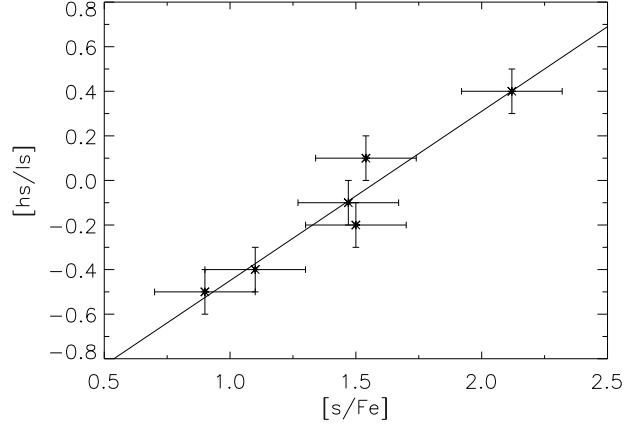


**Fig. 7.** The correlation between the total enrichment of s-process elements ( $[s/Fe]$  which is the mean of  $[Y/Fe]$ ,  $[Zr/Fe]$ ,  $[Ba/Fe]$ ,  $[La/Fe]$ ,  $[Nd/Fe]$  and  $[Sm/Fe]$ ) and the  $[hs/ls]$  index. The straight line gives the simple least-squares fit.

1995), the  $[hs/ls]$  index will not change with increasing dredge-up of enriched material in the stellar envelope, making the  $[hs/ls]$  index independent of the dilution factor of the enriched material by the initial stellar envelope material. The  $[hs/ls]$  correlation with  $[s/Fe]$  therefore reflects a different and more efficient internal nucleosynthesis, with increasing dredge-up efficiency! In AGB evolutionary models, the inclusion of protons into the intershell will create a primary  $^{13}\text{C}$  pocket and induce the neutron production. Fig. 7 indicates therefore that, with increasing dredge-up efficiency, also the dredge-in of protons will increase, giving rise to a higher neutron irradiation.

### 6.3. Metallicity.

Although our sample at this point only consists of 6 objects, a considerable spread in metallicity ranging from  $-0.3$  to  $-1.0$  is observed. Since the  $^{13}\text{C}(\alpha,n)^{16}\text{O}$  neutron source in AGB stars is most likely of primary origin the  $[hs/ls]$  index should increase with decreasing metallicity due to the larger amount of neutrons per iron seed nucleus (e.g. Clayton 1988). This assumes, however, that the diffusion of protons into the C-rich layer itself is independent of metallicity or on parameters linked to the metallicity (like temperature profile, luminosity etc.). A higher neutron exposure is therefore expected for low metallicity objects assuming that the thermal pulse phenomenon itself is independent of metallicity.

In Fig. 8 we display the  $[hs/ls]$ -index in function of the metallicity. The  $21\mu\text{m}$  stars clearly cover a wide range in neutron irradiation in the range of the observed iron abun-

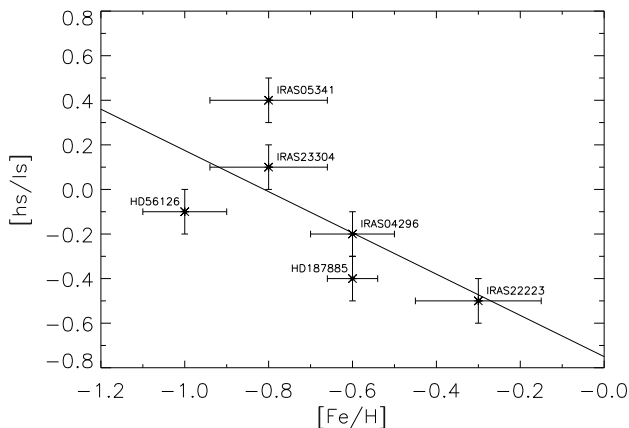


**Fig. 8.** The  $[hs/ls]$  index of the analysed  $21\mu\text{m}$  stars as a function of the metallicity determined by the Fe abundance ( $[Fe/H]$ ). The line gives the simple least-squares fit  $[hs/ls] = -0.93 [Fe/H] - 0.75$ .

is  $-0.67$ ). The most metal deficient object IRAS07134 has seem to have undergone a much smaller neutron irradiation than the less metal deficient IRAS05341. Clearly, also other stellar parameters determine the internal AGB nucleosynthesis during the AGB evolution.

Note that the two stars significantly below the least-square line are the ones for which we detected the very heavy element Hf ( $Z=72$ ). If indeed these high abundances turn out to be true, this would indicate that the s-process is able to produce elements heavier than the Ba peak and thus probably up to the lead-peak! If true, the low  $[hs/ls]$ -index of the two stars might be due to the production of very heavy elements. It is clear that high S/N blue spectra of all the objects are needed for a more detailed discussion.

Moreover, several (probably single) post-AGB objects are known which do not show s-process enrichment nor enhanced C/O ratios. These objects include HD 161796 ( $[Fe/H]=-0.3$ ; Luck et al., 1990), HD 133656 ( $[Fe/H]=-1.0$ ; Van Winckel et al. 1996b) and SAO 239853 ( $[Fe/H]=-0.8$ , Van Winckel 1997) which show very similar metallicities and IR-excesses. Unfortunately, like the  $21\mu\text{m}$  objects they are too far for reliable HIPPARCOS parallaxes so the luminosity differences between the enriched and non-enriched objects is an as yet unknown but probable key parameter in this discussion.

## 7. Comparison with intrinsic and extrinsic enriched stars.

### 7.1. Intrinsic enriched objects: AGB stars

In this section we compare our results on  $21\mu\text{m}$  sources

bert (1985,1986,1990) and Smith et al. (1987) : since the spectra of oxygen rich AGB stars are dominated by strong TiO-bands, only a few spectral windows can be used to infer abundances from atomic lines. The regions in between 740 and 758 nm, and 998 to 1010 nm, were used together with additional IR spectra around 1.6, 2.2 and  $4.0 \mu\text{m}$  to deduce abundances of CNO isotopes. The situation is even worse for C stars where the  $C_2$  and CN bands dominate the optical and IR spectrum. To our knowledge only Utsumi (1985 and references therein) made a quantitative analysis of the s-process enhancement in C stars using two small spectral windows with minimal molecular absorption (475–490 nm, and 440–450 nm). SC stars, on the other hand, are AGB stars with a C/O ratio close to 1.0 making the oxide bands and bands from carbon molecules very weak or absent so that many atomic lines become detectable in the spectrum. We use the results for seven SC stars from a recent paper by Abia & Wallerstein (1998).

In Fig. 9 we compare the observed overabundances of the light s-process elements ( $[ls/Fe]$ ) with the ones observed in intrinsic AGB stars. Since there is strong observational evidence that the  $21\mu\text{m}$  stars are post-carbon stars, it is no surprise that the overabundances of the s-process elements in  $21\mu\text{m}$  stars are indeed large in comparison with MS, intrinsic S and SC stars and are comparable with and on average even slightly higher than observed in C stars. We therefore can confirm earlier results that the increasing C/O ratio in the MS-S-SC-C sequence is also reflected in an increasing enhancement of s-process elements (e.g. Smith & Lambert 1990; Abia & Wallerstein 1998).

### 7.2. Extrinsic enriched objects

To investigate the metallicity dependence of the integrated neutron exposure for intrinsic AGB stars is not easy since the metallicity of field carbon stars is very difficult to determine and the spread in metallicities observed in Galactic M-MS-S-SC stars is not large (e.g. Smith & Lambert 1990). Plez et al. (1993) have shown, however, that seven intrinsic AGB stars in the metal poor ( $[Fe/H] = -0.5$ ) Small Magellanic Cloud do indeed show a very high neutron exposure and they suggest that it is not intrinsic to the SMC but due to the low initial metallicity.

The metallicity spread observed in the extrinsic enriched objects is much larger and there is growing observational evidence that the  $[hs/ls]$  index is indeed anti-correlated with metallicity (e.g. Smith 1999): Busso et al. (1995) confirmed earlier suggestions by Luck & Bond (1991) in a compilation of literature values of the  $[hs/ls]$  index in Ba stars and MS-S stars and quantified tentatively the metallicity dependence of the neutron irradiation as an increase in  $[hs/ls]$  of about 0.2 dex for a metallicity

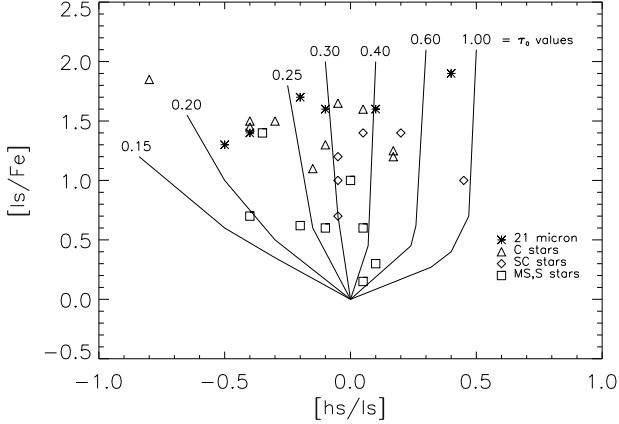


**Fig. 9.** Comparison between the overabundances of light s-process elements observed in the  $21\mu\text{m}$  stars with those from intrinsic AGB stars. 'ls' is the mean of the light s-process elements Y and Zr, while 'hs' is the mean of the heavy s-process elements Ba, La, Nd and Sm. The references for the observations of the intrinsic AGB stars can be found in Abia & Wallerstein (1998). The full lines are the theoretical predictions for different neutron exposures parameterised by  $\tau_0$  (in  $\text{mbarn}^{-1}$ ) are from Busso et al. (1995).

larging the metallicity spread to lower metallicities. North et al. (1994) also found that the  $[\text{hs}/\text{ls}]$  index was correlated with the metallicity in a sample of CH-subgiants. Finally also the low metallicity yellow symbiotics, who recently were included in the Ba-star family, show s-process distributions characterised by a relatively high neutron irradiation (Smith et al. 1996, 1997; Pereira et al. 1998). The results obtained by Luck & Bond (1991) included, however, 4 metal deficient objects with small overabundances showing a very weak neutron irradiation. They dubbed these stars "the metal-deficient Ba stars".

Some caution should be expressed by generalising these results to single star AGB evolution : especially for the short orbital period binaries there is strong evidence that the binarity affects the mass-loss and thus the AGB evolution itself of these binaries. The amount of thermal pulses and the characteristics of the s-process synthesis might therefore also be affected by the orbital elements (e.g. Jorissen & Mayor 1988).

In Fig. 10 we compare the  $[\text{hs}/\text{ls}]$  index in function of the metallicity with the values found in the literature for other s-process enriched objects. This compilation is difficult since the definition of the hs and ls indices is author-dependent. We scaled the abundances to the definition given in section 4.4. For undetermined abundances of the CH giants, we used the tables of Malanek (1987) with a

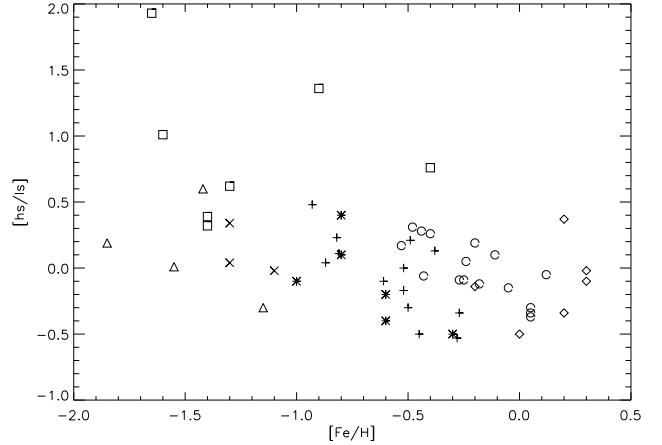


**Fig. 10.** The  $[\text{hs}/\text{ls}]$  index as a function of the metallicity for a sample of s-process enriched objects. Asterisks are the  $21\mu\text{m}$  stars; triangles the metal deficient Barium stars from Luck & Bond 1991; squares the CH-giants from Vanture (1992); circles the Ba-stars from the compilation made by Busso et al. (1995); plus-signs the CH-subgiants from North et al. (1994); crosses the yellow symbiotic stars from Smith et al. (1996,1997) and Pereira et al. (1998); diamonds the SC stars from Abia & Wallerstein (1998).

in total 7 elements (Sr, Y, Zr, Ba, La, Nd and Sm) were available.

Fig. 10 shows that there is a large spread in the integrated neutron irradiation, but that there is indeed a global increase with decreasing metallicities from  $[\text{Fe}/\text{H}] \sim -0.5$  downwards as already noted by several authors (e.g. Smith, 1999). Three out of four "metal-deficient Ba stars" show a very low  $[\text{hs}/\text{ls}]$ -index (Luck & Bond, 1991). These stars certainly are worth a re-analysis based on higher resolution, higher signal-to-noise spectra since the internal errors of the analysis based on photographic intermediate resolution ( $0.2 \text{ \AA}$ ) spectra are rather large and the observed overabundances small (Luck & Bond, 1991). Some CH-stars show extremely high  $[\text{hs}/\text{ls}]$ -indices for their metallicity but also some Ba stars like the very Nd-rich HD 35155 (not in the figure) show atypical values. The  $21\mu\text{m}$  post-AGB objects follow the same trend as the CH-subgiants of the same metallicity and show on average a somewhat lower  $[\text{hs}/\text{ls}]$ -index compared to the Ba giants.

We can conclude that the metallicity dependence of the neutron exposure has a large *intrinsic* spread which confirms that certainly also other fundamental parameters determine the internal nucleosynthesis and dredge-up phenomena during the AGB evolution.

With their low metallicity ( $[\text{Fe}/\text{H}]$  ranging from  $-0.3$  to  $-1.0$ ), high C/O ratio (ranging from 1.0 to 2.9) and especially their high photospheric abundance of s-process elements, we confirm that they are post-3rd-dredge-up objects. Since also the circumstellar environment is C-rich and no orbital motion is observed we can classify the  $21\mu\text{m}$  stars as single post-carbon stars of low initial mass.

The G-F spectral type makes that a wide variety of s-process elements can be detected by their atomic lines. This, together with their significant spread in metallicity, make that the  $21\mu\text{m}$  stars are ideal objects to constrain the AGB nucleosynthesis and dredge-up models. The most interesting constraint in this context comes from the possibility to accurately determine a wide variety of elemental abundances of these intrinsically enriched objects. Contrary to AGB stars themselves, no photospheric molecular absorption is observed, so isotopic ratios of key elements are in the  $21\mu\text{m}$  stars unfortunately difficult to determine. The molecular bands originating in the circumstellar environment can, however, be used for some isotopes like  $^{12}\text{C}$  and  $^{13}\text{C}$  (e.g. Bakker & Lambert 1998a).

We can summarise the main conclusions with respect to the s-process nucleosynthesis displayed by  $21\mu\text{m}$  stars as follows :

- The  $21\mu\text{m}$  stars display a wealth of atomic lines from s-process elements. The photospheric spectrum of stars like IRAS05341 is even completely dominated by atomic lines of heavy elements. The observed overabundances of s-process elements in the analysed  $21\mu\text{m}$  stars are large and range from  $[\text{ls}/\text{Fe}] = +1.3$  to  $+1.9$  which make the  $21\mu\text{m}$  stars among the most s-process enriched objects known.
- The  $21\mu\text{m}$  stars display a wide variety of integrated neutron irradiation as parameterised by the observational  $[\text{hs}/\text{ls}]$ -index, corresponding to a  $\tau_0$  neutron exposure from  $\tau_0 = 0.2$  to  $0.8 \text{ mbarn}^{-1}$ .
- The  $[\text{hs}/\text{ls}]$  index displayed by the  $21\mu\text{m}$  stars is strongly correlated (classical correlation coefficient of  $+0.96$ ) with the total enrichment of the s-process elements as parameterised by the  $[\text{s}/\text{Fe}]$ -index, in the sense that more enriched objects also display a higher integrated neutron irradiation. Since in carbon stars the asymptotic values of the s-process distribution is probably reached, this means that the dredge-up efficiency is strongly linked with the neutron production in the intershell !
- The anti correlation of the  $[\text{hs}/\text{ls}]$  index with the metallicity of the  $21\mu\text{m}$  objects is less well determined (classical correlation coefficient  $-0.67$ ) and contains a large scatter. This scatter is certainly intrinsic and confirms that also other fundamental parameters determine the internal nucleosynthesis and dredge-up

- Compared with other s-process enriched objects of extrinsic nature, the neutron exposure displayed by the  $21\mu\text{m}$  stars fall roughly in the same range as the CH subgiants and is on average lower than it is in Ba-giants of the same metallicity. Note that the metallicity dependence of the neutron exposure displayed by intrinsic and extrinsic objects contains also a large intrinsic scatter. Especially the iron deficient Ba stars as defined by Luck & Bond (1991) should be analysed in great detail since they display a very low neutron irradiation for their low metallicity.

We can conclude that a homogeneous detailed study of the  $21\mu\text{m}$  stars forms a very useful complement to other types of s-process enriched objects (intrinsic AGB stars and extrinsic enriched objects) used in the observational study of the theoretically less well understood s-process nucleosynthesis, mass-loss and dredge-up phenomena occurring on the AGB.

*Acknowledgements.* The authors would like to thank the staff of the NTT and WHT telescopes for the welcome support during the observations. It is a pleasure to acknowledge the Vienna Atomic Line Database (VALD2) for the usefull data-set and Prof. Kurucz for the distribution of his software. Also Eric Bakker is warmly acknowledged for providing some of the spectra as well as Christoffel Waelkens and Nami Mowlavi for stimulating discussions. HVW and MR acknowledge support from the Fund of Scientific Research, Flanders.

## References

- Abia C., Wallerstein G., 1998, MNRAS 293, 89
- Bakker E.J., Lambert D.L., 1998a, ApJ 502, 417
- Bakker E.J., Lambert D.L., 1998b, ApJ 508, 387
- Bakker E.J., Waters L.B.F.M., Lamers H.J.G.L.M., et al., 1996, A&A 310, 893
- Bakker E.J., Van Dishoeck E.F., Waters L.B.F.M., Schoenmaker T., 1997, A&A 323, 469
- Biehl D., 1976, PhD thesis, Univ. Kiel
- Biémont E., Hibbert A., Godefroid M., Vaeck N., Fawett B.C., 1991, ApJ 375, 818
- Biémont E., Hibbert A., Godefroid M., Vaeck N., 1993, ApJ 412, 431
- Blackwell D.E., Shallis M.J., Simmons G.J., 1980, A&A 81, 340
- Bujarrabal V., Alcolea J., Planesas P., 1992, A&A 257, 701
- Busso M., Gallino R., Lambert D.L., Raiteri C.M., Smith V.V., 1992, ApJ 399, 218
- Busso M., Lambert D.L., Beglio L., et al., 1995, ApJ 446, 775
- Clayton D.D., 1988, MNRAS 234, 1
- Cowley C.R., Downs P.L., 1980, ApJ 236, 648
- Dayal A., Hoffmann W.F., Biegging J.H., et al., 1998, ApJ 492, 603
- Decin L., Van Winckel H., Waelkens C., Bakker E.J., 1998, A&A 332, 222

- Fuhr J.R., Martin G.A., Wiese W.L., 1988, *Journal of Physical and Chemical Reference Data*, Volume 17, Supplement No. 4
- Gallino R., Arlandini C., Busso M., et al., 1998, *ApJ* 497, 38
- Geballe T.R., Van Der Veen W.E.C.J., 1990, *A&A* 235, L9
- Gonzalez G., Lambert L., Giridhar S., 1997, *ApJ* 481, 452
- Grevesse N., 1989, in *AIP Conferences Series 183 : "Cosmochemical Abundances of Matter"*, ed C.J. Waddington, American Institute of Physics, New York, p.9
- Herwig F., Bloeker T., Schönberner D., El Eid M., 1997, *A&A* 324, L81
- Hibbert A., Biémont E., Godefroid M., Vaecck N., 1991, *A&ASS* 88, 505
- Hibbert A., Biémont E., Godefroid M., Vaecck N., 1993, *A&ASS* 99, 179
- Hrivnak B.J., 1995, *ApJ* 438, 341
- Hrivnak B.J., Kwok S., 1999, *ApJ* 513, 869
- Hrivnak B.J., Langill P.P., Su H.Y.L., Kwok S., 1999, *ApJ* 513, 421
- Jorissen A., 1999, in : *IAU Symp. 191 "AGB stars"*, Le Bertre T., Lèbre A., Waelkens C. (eds.), 437
- Jorissen A., Arnould M., 1989, *A&A* 221, 161
- Jorissen A., Mayor M., 1988, *A&A* 198, 187
- Jorissen A., Frayer D.T., Johnson H.R., Mayor M., Smith V.V., 1993, *A&A* 271, 463
- Justtanont K., Barlow M.J., Skinner C.J., et al., 1996, *A&A* 309, 612
- Klochkova V.G., 1995, *MNRAS* 272, 710
- Klochkova V.G., Szczerba R., Panchuk V.E., Volk K., 1999, *A&A* 345, 905
- Knapp G.R., Sutin B.M., Phillips T.G., et al., 1989, *ApJ* 336, 822
- Kupka F., Piskunov N.E., Ryabchikova T.A., Stempels H.C., Weiss W.W., 1999, *A&A* submitted
- Kurucz R.L., 1993, CD-ROM set, Cambridge, MA : Smithsonian Astrophysical Observatory
- Kwok S., Volk K.M., Hrivnak B.J., 1989, *ApJ* 345, 51
- Kwok S., Hrivnak B.J., Geballe T.R., 1995, *ApJ* 454, 394
- Kwok S., Volk K., Hrivnak B.J., 1999, in : *IAU Symp. 191 "AGB stars"*, Le Bertre T., Lèbre A., Waelkens C. (eds.), 297
- Lambert D.L., 1989, in *AIP Conferences Series 183 : "Cosmochemical Abundances of Matter"*, ed C.J. Waddington, American Institute of Physics, New York, p.168
- Lambert D.L., Smith V.V., Busso M., Gallino R., Straniero O., 1995, *ApJ* 450, 302
- Lambert D.L., Heath J.E., Lemke M., Drake J., 1996, *ApJ* 103, 183
- Langer N., Heger A., Wellstein S., Herwig F., 1999, *A&A* 346, L37
- Lèbre A., Maunon N., Gillet D., Barthes D., 1996, *A&A* 310, 923
- Likkel L., 1989, *ApJ* 344, 350
- Likkel L., Forveille T., Omont A., Morris M., 1991, *A&A* 246, 153
- Luck R.E., Bond H.E., 1991, *ApJS* 77, 515
- Luck R.E., Bond H.E., Lambert D.L., 1990, *ApJ* 357, 188
- McWilliam A., 1997, *ARA&A* 35, 503
- McWilliam A., Preston G.W., Sneden C., Searle L., 1995, *AJ* 109, 2757
- Meixner M., Skinner C.J., Graham J.R., et al., 1997, *ApJ* 482, 897
- Mowlavi N., 1999, *A&A* 344, 617
- Mowlavi N., Jorissen A., Arnould M., 1998, *A&A* 311, 803
- North P., Berthet S., Lanz T., 1994, *A&A* 281, 775
- Omont A., Loup C., Forveille T., et al., 1993, *A&A* 267, 515
- Oudmaijer R.D., Bakker E.J., 1994, *MNRAS* 271, 615
- Parthasarathy M., Garcia Lario P., Pottasch S.R., 1992, *A&A* 264, 159
- Pereira C.B., Smith V.V., Cunha K., 1998, *AJ* 116, 1977
- Plez B., Smith V.V., Lambert D.L., 1993, *ApJ* 418, 812
- Reader J., Corliss C.H., Wiese W.L., Martin G.A., 1980, *NSRDS-NBS* 68, 1
- Reddy B.E., Parthasarathy M., 1996, *AJ* 112, 2053
- Reddy B.E., Parthasarathy M., Gonzalez G., Bakker E.J., 1997, *A&A* 328, 331
- Smith V.V., 1984, *A&A* 132, 326
- Smith V.V., 1999, in : *IAU symp. 191 "AGB stars"*, Le Bertre T., Lèbre A., Waelkens C. (eds.), ASP conference series, 69
- Smith V.V., Lambert D.L., 1985, *ApJ* 294, 326
- Smith V.V., Lambert D.L., 1986, *ApJ* 311, 843
- Smith V.V., Lambert D.L., 1990, *ApJS* 72, 387
- Smith V.V., Lambert D.L., McWilliam A., 1987, *ApJ* 320, 862
- Smith V.V., Cunha K., Jorissen A., Boffin H.M.J., 1996, *A&A* 315, 179
- Smith V.V., Cunha K., Jorissen A., Boffin H.M.J., 1997, *A&A* 324, 97
- Straniero O., Gallino R., Busso M., et al., 1995, *ApJ* 440, L85
- Thévenin F., 1989, *A&AS* 77, 137
- Thévenin F., 1990, *A&AS* 82, 179
- Ulrich R.K., 1973, in : D.N. Schramm & W.S. Arnett (eds) *Explosive Nucleosynthesis*. Austin. University of Texas Press, p. 139
- Utsumi K., 1985, in : M. Jashek & P.L. Keenan (eds) *Cool Stars with Excesses of Heavy Elements*. Reidel, Dordrecht, p. 243
- Van Eck S., Jorissen A., Udry S., Mayor M., Pernier B., 1998, *A&A* 329, 971
- Vanture A.D., 1992, *AJ* 104, 1997
- Van Winckel H., 1997, *A&A* 319, 561
- Van Winckel H., 1999, in : *IAU Symp. 191 "AGB stars"*, Le Bertre T., Lèbre A., Waelkens C. (eds.), 465
- Van Winckel H., Waelkens C., Waters L.B.F.M., 1996a, *A&A* 306, L37
- Van Winckel H., Oudmaijer R.D., Trams N.R., 1996b, *A&A* 312, 553
- Venn K.A., 1995, *ApJS* 99, 659
- Volk K., Kwok S., Hrivnak B.J., 1999, *ApJ* 516, L99
- Wheeler J.C., Sneden C., Truran J.W.Jr., 1989, *ARA&A* 27, 279
- Wiese W.L., Smith M.W., Glennon B.M., 1966, *NSRDS-NBS*, Vol I, 4
- Woodsworth A.W., Kwok S., Chan S.J., 1990, *A&A* 228, 503
- Začs L., Klochkova V.G., Panchuk V.E., 1995, *MNRAS* 275, 764